The Cryosphere

Mechanisms influencing seasonal to inter-annual prediction skill of sea ice extent in the Arctic Ocean in MIROC

Jun Ono[1], **Hiroaki Tatebe**[1], **Yoshiki Komuro**[1], **Masato I. Nodzu**[2], and **Masayoshi Ishii**[3]

[1]Japan Agency for Marine-Earth Science and Technology, Yokohama, 236-0001, Japan
[2]Tokyo Metropolitan University, Hachioji, 192-0397, Japan
[3]Meteorological Research Institute, Japan Meteorological Agency, Tsukuba, 305-0052, Japan

Correspondence: Jun Ono (jun.ono@jamstec.go.jp)

Abstract. To assess the skill of seasonal to inter-annual predictions of the detrended sea ice extent in the Arctic Ocean (SIE_{AO}) and to clarify the underlying physical processes, we conducted ensemble hindcasts, started on 1 January, 1 April, 1 July and 1 October for each year from 1980 to 2011, for lead times up to three years, using the Model for Interdisciplinary Research on Climate (MIROC) version 5 initialised with the observed atmosphere and ocean anomalies and sea ice concentration. Significant skill is found for the winter months: the December SIE_{AO} can be predicted up to 11 months ahead (anomaly correlation coefficient is 0.42). This skill might be attributed to the subsurface ocean heat content originating in the North Atlantic. A plausible mechanism is as follows: the subsurface water flows into the Barents Sea from spring to fall and emerges at the surface in winter by vertical mixing, and eventually affects the sea ice variability there. Meanwhile, the September SIE_{AO} predictions are skillful for lead times of up to two months, due to the persistence of sea ice in the Beaufort, Chukchi, and East Siberian seas initialised in July, as suggested by previous studies.

1 Introduction

The Arctic has warmed more than twice as much as the global average (e.g., Bekryaev et al., 2010; Cohen et al., 2014), this is referred to as Arctic amplification. Sea ice reduction resulting from climate change is one of the main processes contributing to Arctic amplification (e.g., Pithan and Mauritsen, 2014). Arctic summer sea ice extent has declined at about 14 % per decade (National Snow and Ice Data Cen-

ter, 2016, http://nsidc.org/arcticseaicenews/). In September 2012, sea ice extent reached its minimum since satellite observations began in the late 1970s. Moreover, Arctic sea ice thickness has decreased by around 65 % from 1975 to 2012 (Kwok et al., 2009; Lindsay and Schweiger, 2015).

In contrast to the rapid warming in the Arctic, severely cold winters have occurred more frequently at midlatitudes. Although the exact cause is still being debated (e.g., Barnes and Screen, 2015), Mori et al. (2014) have shown, using ensemble experiments with an atmospheric general circulation model, that the more frequent cold winters at midlatitudes can be partly explained by the sea ice decrease in the Barents and Kara Seas. Therefore, further investigation of the mechanisms driving Arctic sea ice variability is of great importance for more accurate projections of climate change, not only in the Arctic but also for the midlatitudes.

A previous study based on two and five year perfect-model experiments from 1 January and 1 September has shown that the potential predictability for sea ice extent remains statistically significant at lead times up to 1–2 years. This is primarily because of the persistence of ice thickness anomalies from summer to summer and the persistence of sea surface temperature anomalies from the melt to growth seasons (Blanchard-Wrigglesworth et al., 2011a; Guemas et al., 2014). These features are also found in the results of experiments comparing multiple climate models (Day et al., 2014b; Tietsche et al., 2014). The observed detrended Arctic sea ice extent, based on ensemble hindcasts can be predicted up to 2–7 and 5–11 months ahead for summer and winter, respectively (e.g., Chevallier et al., 2013; Sigmond et al., 2013; Wang et al., 2013; Msadek et al., 2014; Peterson et al., 2015; Guemas

et al., 2016; Sigmond et al., 2016). In these ensemble hindcasts, it is found that ice thickness and surface or subsurface water temperatures are closely related to the prediction skill, as suggested by idealised or perfect-model experiments with climate models (e.g., Blanchard-Wrigglesworth et al., 2011b; Chevallier and Salas y Mélia, 2012; Day et al., 2014a).

Until very recently, the mechanisms by which the above variables contribute to the prediction skill had not been quantified. Bushuk et al. (2017) examined the physical mechanisms underlying the prediction skill of regional sea ice extent and showed for the first time the importance of the initialisations of ocean subsurface temperatures and sea ice thickness in their dynamical prediction system.

Motivated by the above studies, we first conduct initialised ensemble hindcasts, using a climate model to assess the seasonal to inter-annual predictability of sea ice extent in the Arctic Ocean, and further investigate sources for prediction skill and clarify the physical processes linking the prediction skill to its sources. In particular, the present study reveals that subsurface ocean heat content originating from the North Atlantic contributes to the predictability of winter sea ice through advection and vertical mixing processes, which is somewhat different from the re-emergence process of the local subsurface ocean temperature suggested by Bushuk et al. (2017).

2 Experimental design

The climate model used here is a low-resolution version of the Model for Interdisciplinary Research on Climate, version 5 (MIROC5) (Watanabe et al., 2010), which contributed to the fifth phase of the Coupled Model Intercomparison Project and the Intergovernmental Panel on Climate Change Fifth Assessment Report (IPCC, 2013). The atmospheric component has a horizontal resolution of T42 spectral truncation (approximately 2.8°) and comprises 40 vertical layers up to 3 hPa. The oceanic component has horizontal resolutions of 1.4° in longitude and 0.5–1.4° in latitude, and comprises 50 vertical layers. The sea ice component of MIROC5 contains one-layer thermodynamics (Bitz and Lipscomb, 1999), elastic–viscous–plastic rheology (Hunke and Dukowicz, 1997), and the subgrid ice thickness distribution (Bitz et al., 2001) with five categories; the detailed structure has been described in Komuro et al. (2012).

To initialise MIROC5, we adopted anomaly assimilation for the atmosphere and ocean and full-field assimilation for sea ice. Anomalies were calculated as the deviations from the climatology defined in the 1961–2000 period. The observed 6-hourly air temperature and wind vectors from the 55-year Japanese Reanalysis (JRA-55) dataset (Kobayashi et al., 2015) were linearly interpolated to the atmospheric model's grid. The observed monthly ocean temperature, salinity, and sea ice concentration (SIC) from the gridded monthly objective analysis produced by Ishii et al. (2006) and Ishii

and Kimoto (2009) were linearly interpolated to obtain the daily values, and the same grid as the ocean model. The ocean data are based on the latest observational databases: the World Ocean Database (WOD05), the World Ocean Atlas (WOA05), and the Global Temperature Salinity Profile Program (GTSPP) provided by the U.S. National Oceanographic Data Center (NODC); and a sea surface temperature (SST) analysis, in particular centennial in situ observation based estimates of variability of SST and marine meteorological variables (COBE SST; Ishii et al., 2005; Hirahara et al., 2014). The SIC data are based on satellite observations from the Nimbus-5 Scanning Multichannel Microwave Radiometer (SMMR), the Special Sensor Microwave Imager (SSM/I), and the Special Sensor Microwave Imager/Sounder (SSMIS; Armstrong et al., 2012).

In the assimilation runs, the atmospheric anomalies were assimilated into MIROC5 below 100 hPa at 6-hourly intervals and the oceanic anomalies above 3000 m depth at one-day intervals except in sea ice regions, using a modified incremental analysis update scheme (Tatebe et al., 2012). Meanwhile, SIC was assimilated at 1-day intervals following Lindsay and Zhang (2006) and Stark et al. (2008). These assimilations were conducted over the period 1975–2011 with eight ensemble members produced by perturbing the sea surface temperature based on observational errors. The atmospheric and oceanic initial states were obtained from a non-initialised twentieth-century run with historical natural and anthropogenic forcings.

On the basis of the assimilation runs, the hindcast experiments were integrated for 3 years from 1 January, 2 years and 9 months from 1 April, 2 years and 6 months from 1 July and 2 years and 3 months from 1 October for each year from 1980 to 2011. The initial state of the atmosphere and ocean was obtained from the corresponding assimilation runs. In addition, a control run with MIROC version 5.2, a minor update of MIROC5, was used to interpret the physical processes contributing to the prediction skill in the hindcasts. This simulation was run with external forcings fixed at the levels of the year 2000 under a multi-model inter-comparison project (Day et al., 2016).

In Sects. 3 and 4, we analyse the detrended monthly anomalies to extract internal variations in seasonal to inter-annual timescales. Here, the detrended components were calculated by subtracting monthly linear trends during 1980–2009 from the original monthly data, and anomalies are defined as deviations from the climatology from 1980–2009. Moreover, climate drifts in the hindcasts are removed according to the International Clivar Project Office (ICPO, 2011). Here, the climate drift T_{drf} is estimated as follows:

$T_{\mathrm{drf}}(\tau) = \frac{1}{N} \sum_{k=1}^{N} (T_{\mathrm{p}}^{k}(\tau) - T_{\mathrm{a}}^{k}(\tau))$, where $k = 1, \cdots, N$ is the initial time; τ is the forecast lead time; T is the monthly quantity of interest, for example the temperature and sea ice concentration; and the subscripts "p" and "a" represent
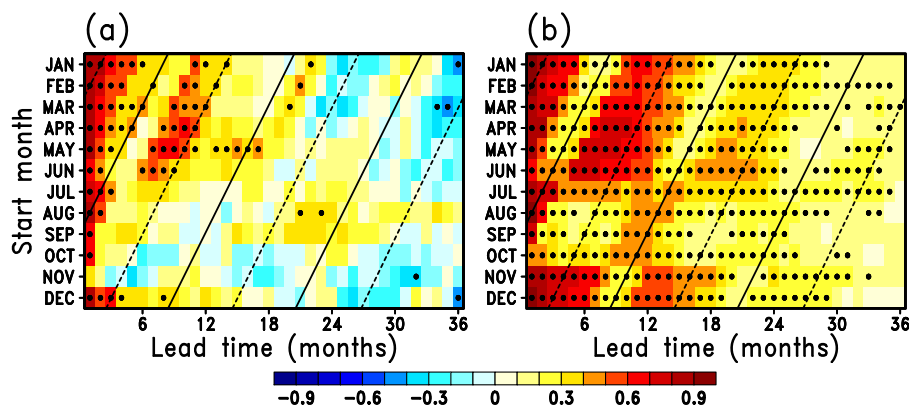
Figure 1. Lagged auto-correlation coefficients of the detrended SIE$_{AO}$ anomaly derived from **(a)** observations (Ishii et al., 2006; Ishii and Kimoto, 2009) and **(b)** a model control simulation, for each start month, against lead time, following Day et al. (2014b). Solid and dashed lines denote values for the September and March target months, respectively. Black dots indicate statistical significance at a 95 % confidence level based on a two-sided Student's t test with 30 and 200 degrees of freedom in the observations and model, respectively.

the ensemble averaged prediction and the corresponding assimilation, respectively. As mentioned in Sect. 1, sea ice reduction in the Arctic Ocean, especially in the Barents and Kara Seas, could lead to extreme weather at midlatitudes, which may be related to the warming of the Arctic Ocean interior (e.g., Polyakov et al., 2012). To clearly interpret the physical mechanisms influencing sea ice extent in the Arctic Ocean (hereafter SIE$_{AO}$), SIE$_{AO}$ is defined from the cumulative area for all grid cells north of 65° N with SIC greater than 15 %. From this definition, Baffin Bay and Hudson Bay are partially included in the domain, but the directions of the main currents are from the Arctic Ocean interior (shelves and basins) to Baffin Bay through the straits of the Canadian Arctic Archipelago (e.g., Aksenov et al., 2011). Thus, the direct impacts of Baffin Bay and Hudson Bay on the Arctic Ocean interior are considered to be small. Note that the results of this study are not directly comparable with other hindcast studies that focus on pan-Arctic SIE (e.g., Chevallier et al., 2013; Sigmond et al., 2013; Wang et al., 2013; Msadek et al., 2014; Peterson et al., 2015; Guemas et al., 2016; Sigmond et al., 2016), due to the choice of Arctic Ocean domain. For comparison, the results for the detrended sea ice extent anomaly in the Northern Hemisphere are shown in the supporting information.

3 Predictability of Arctic sea ice extent

We first examine the potential predictability of SIE$_{AO}$ (Fig. 1), based on the lagged auto-correlation coefficients, which is the skill of the persistence forecast. The lagged correlations with the observations (Ishii et al., 2006; Ishii and Kimoto, 2009) decrease within the first few months for all of the start months, and those originating between January and June subsequently rise again in the winter (November through March). Significant skill in the control run is

obtained for greater lead times than in the observations, which is consistent with previous studies (e.g., Blanchard-Wrigglesworth et al., 2011b; Day et al., 2014b). For the SIE in the Northern Hemisphere (Fig. S1a in the Supplement), the correlation patterns are similar to those in Day et al. (2014b), except for a lead time of one month for May which may be due to differences in the observational time period (Fig. S1d). However, the reemergence in winter is weaker than that for SIE$_{AO}$. This is because the winter SIE$_{AO}$ variability is dominated by changes in the Barents and Greenland–Icelandic–Norwegian (GIN) seas, which have long persistence timescales relative to other regions of winter sea ice variability.

We next evaluate the SIE$_{AO}$ prediction skill (Fig. 2a and b), with the anomaly correlation coefficient (ACC) and the root-mean-square error (RMSE) between the detrended observations and the hindcasts (e.g., Wang et al., 2013). Here, the RMSE values are normalised by the standard deviation of each month. In the hindcasts started from 1 July, the ACC for September is statistically significant and exceeds that of the persistence forecast, suggesting that September SIE$_{AO}$ can be dynamically predicted from the previous July (ACC = 0.79). Although the significance of the ACC is borderline, the results suggest that September SIE$_{AO}$ is potentially predictable from 1 April (ACC = 0.37), which is consistent with the results of Peterson et al. (2015). The ACC is also significant for the winter SIE$_{AO}$, in particular for December, except for the hindcasts started from 1 April, indicating the potential use of dynamical forecasts up to 11 months ahead (ACC = 0.42). The RMSE values for the first several lead months are smaller than the standard deviation for all hindcasts. The time series of September SIE$_{AO}$ shows that both the assimilation and hindcasts capture the observed interannual variability, although the model underestimates the variability in the mid-1980s and mid-1990s (Fig. 2c). The
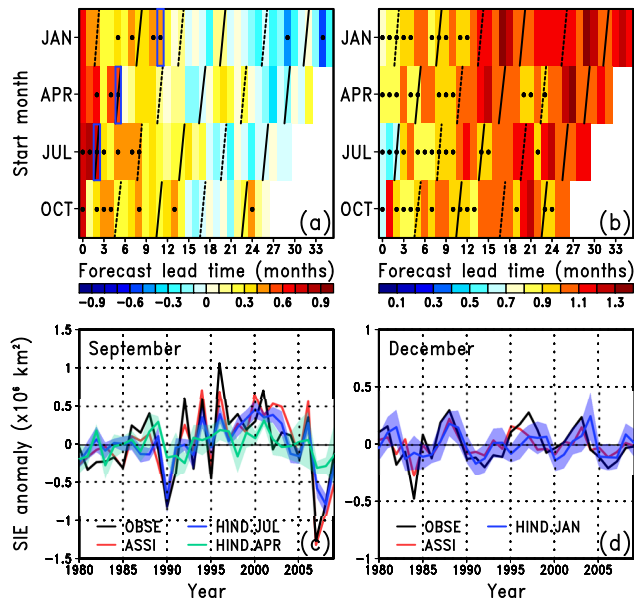
Figure 2. Lead time dependence of **(a)** SIE_{AO} ACC and **(b)** SIE_{AO} RMSE ($\times 10^6$ km^2) for January, April, July, and October start hindcasts. The SIE_{AO} ACC scores of hindcasts, which are higher than those of the persistence forecast and statistically significant at the 95 % confidence level based on a two-sided Student's t test, are denoted by black dots. The SIE_{AO} RMSE scores, which are normalised by the standard deviation, are denoted by black dots if the values are less than 1.0. Boxes in **(a)** indicate the lead time of the time series shown in **(c)** and **(d)**. Time series of the detrended SIE_{AO} anomaly for **(c)** September and **(d)** December, from the observations (OBSE; black line), assimilation (ASSI; red line), and hindcasts started from 1 July and 1 January (HIND.JUL and HIND.JAN; blue line). HIND.JUL is the September SIE_{AO} at 2 months lead time and HIND.JAL is the December SIE_{AO} at 11 months lead time. Blue shading indicates the ensemble spread. In **(c)**, the September SIE_{AO} at 5 months lead time, started from 1 April (HIND.APR), is superimposed by an aqua line and shading.

observed SIE_{AO} in December is contained within the ensemble spread, excluding the mid-1980s (Fig. 2d). We also show the same figure as Fig. 2 in Fig. S2, except that the detrended sea ice extent anomaly is calculated for the Northern Hemisphere. The lower ACC at short lead times for the hindcasts started from January and April (Fig. S2a) may be due to the lower ACC and higher RMSE for sea ice concentration in the Sea of Okhotsk, the Bering Sea, and the Labrador Sea (not shown). The RMSE values in winter are large (Fig. S2b) compared to Fig. 2b because SIE_{AO} does not include the area where sea ice variability is large. The differences between Fig. 2d and Fig. S2d are also due to the effect of the domain choice.

4   Possible mechanisms for prediction skill

Focusing on both the hindcasts started from 1 January, in which the December SIE_{AO} has high skill even at long lead times, and those started from 1 July, in which the September SIE_{AO} is significant, we examine mechanisms for the prediction skill. Figure 3 shows the lagged cross-correlation between the SIE_{AO} and the sea ice volume in the Arctic Ocean (SIV_{AO}), and those between SIE_{AO} and ocean heat content in the Arctic Ocean (OHC_{AO}) for the control run as well as the hindcasts started from January and July. Here, the SIV_{AO} is defined as the sum of the grid cell volumes obtained by multiplying the sea ice thickness (SIT) by the SIC and the area for grid cells with SIC greater than 15 % and the OHC_{AO} is the vertically integrated temperature multiplied by the density and specific heat capacity of seawater from the surface to a depth of 200 m, in the same area as the SIE_{AO}.

The SIV_{AO} has stronger positive correlations with the SIE_{AO} in summer than in winter (Fig. 3a–c), which is consistent with Chevallier and Salas y Mélia (2012). Conversely, the OHC_{AO} has more persistent negative correlations with the SIE_{AO} in winter than in summer (Fig. 3d–f). In the hindcasts started from 1 January, the December SIE_{AO} is significantly correlated with the OHC_{AO} from January to December. Similar features can be seen in the hindcasts started from 1 July. The SIE_{AO} in September is significantly correlated with the SIV_{AO} in July for both of the hindcasts, but only weakly correlated with the OHC_{AO}. Thus, sources for the prediction skill of the December and September SIE_{AO} are suggested to be the ocean heat content from the surface to a depth of 200 m after January, and the sea ice states in July. For the sea ice extent anomaly calculated in the Northern Hemisphere (Fig. S3), the patterns of the lagged correlation coefficients are broadly similar to those in Fig. 3. However, the correlations between the SIE and SIV are higher than those in the Arctic domain north of 65° N. One reason might be the contribution of sea ice variability south of 65° N. In addition, the correlations between SIE and OHC show weak positive values from June to October in the hindcasts. This is partly because the OHC includes the regions where sea ice does not exist throughout the year.

We next clarify the physical processes linking the prediction skill to the sources of that skill. Figure 4 shows the SIC, SIT, and OHC north of 60° N regressed on the model-predicted December SIE_{AO}. The most significant signals for both SIC and SIT are found in the Barents Sea (BS) of the Arctic Ocean (Fig. 4a and b). It is well known that winter sea ice variability in the BS dominates that in the Arctic Ocean (e.g., Smedsrud et al., 2013), which is consistent with our results. At a lag of 9 months (Fig. 4c), negative correlation and regression coefficients for the OHC are found in regions from the northern part of the GIN seas to the western part of the BS. The signals become strong in the western part of the BS at a lag of 6 months (Fig. 4d), further extend across the entire BS at a lag of 3 months (Fig. 4e) and still appear in the
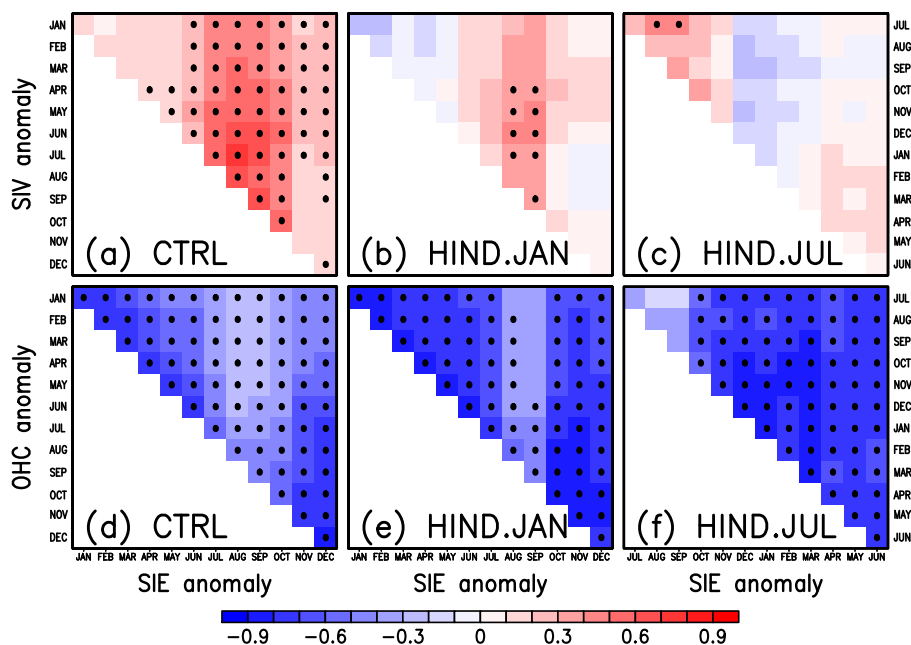
Figure 3. Lagged correlation coefficients between the detrended SIE_{AO} anomaly, **(a–c)** the detrended SIV_{AO} anomaly and **(d–f)** the detrended OHC_{AO} anomaly. Left, middle, and right panels indicate values obtained from the control run (CTRL), the hindcasts started from 1 January (HIND.JAN), and the hindcasts started from 1 July (HIND.JUL), respectively. Black dots indicate statistical significance at the 95 % confidence level based on a two-sided Student's t test with 30 and 200 degrees of freedom in the observations and model. Note that the horizontal and vertical axes in the hindcasts started from 1 July are different from those in the control run and the hindcasts started from 1 January.

BS at a lag of zero (Fig. 4f). These features are also found in the control run (Fig. S4), suggesting that the physical processes in the hindcasts are not due to processes distorted by the influence of initialisation or climate drift in MIROC5. In contrast, the December SIE_{AO} cannot be predicted from 1 April (Fig. 2a), although significant regression and correlation coefficients appear in the results for the April hindcasts (Fig. S5). This may be because the RMSE for April SIC in the BS is larger in the April hindcasts than the January hindcasts (not shown). In this study, since we do not assimilate ocean data beneath the sea ice, initialised ocean states underneath the sea ice are considered to be different from the real ocean. Particularly, in the BS where sea ice variability is related to the skillful prediction of December SIE_{AO}, standard deviation of sea ice is larger in April than in January, and thus the initial shock might be large in April.

Considering that the Norwegian Atlantic Current tends to flow into the BS (e.g., Polyakov et al., 2005), the North Atlantic might be the source the OHC anomaly, contributing to the significant skill of the December SIE_{AO}. A plausible mechanism is as follows: the OHC anomalies initialised in the North Atlantic that flow into the BS through advection, subsequently emerge at the surface due to vertical mixing in winter, and affect the December sea ice distribution in the BS and eventually in the Arctic Ocean. This hypothesis is partly supported by Nakanowatari et al. (2014). As originally pro-

posed by Bushunk et al. (2017), our results suggest that the initialisation of subsurface ocean temperature contributes to the skillful prediction of the winter sea ice extent in the BS.

For September, the sea ice states initialised in July persist until September in the Beaufort, Chukchi, and East Siberian Seas (Fig. 5), which is consistent with Bushuk et al. (2017). Consequently, this persistence contributes to the prediction skill of the September SIE_{AO}. In the hindcasts started from 1 April, the September SIE_{AO} shows similar lagged correlation patterns to the July hindcasts for SIV_{AO} (Fig. S6a) and OHC_{AO} (Fig. S6b). Thus, the same physical processes as the July hindcasts are expected to be present in the April hindcasts. However, the positive regression and correlation patterns for SIC and SIT are lower than those for the July hindcasts, particularly in the Pacific Sector of the Arctic Ocean (Fig. S6c and d). In contrast, similar patterns to Fig. 5 clearly appear in the Pacific sector of the Arctic Ocean for the control experiment (Fig. S7). These results suggest that the persistence of sea ice contributes to the skill of September SIE_{AO} started from 1 April, but errors in the initial conditions for SIT and model drift may lead to unclear signals in Fig. S6.

5 Concluding remarks

We investigated the predictability of the detrended SIE_{AO} anomaly and its sources based on an ensemble of hind-
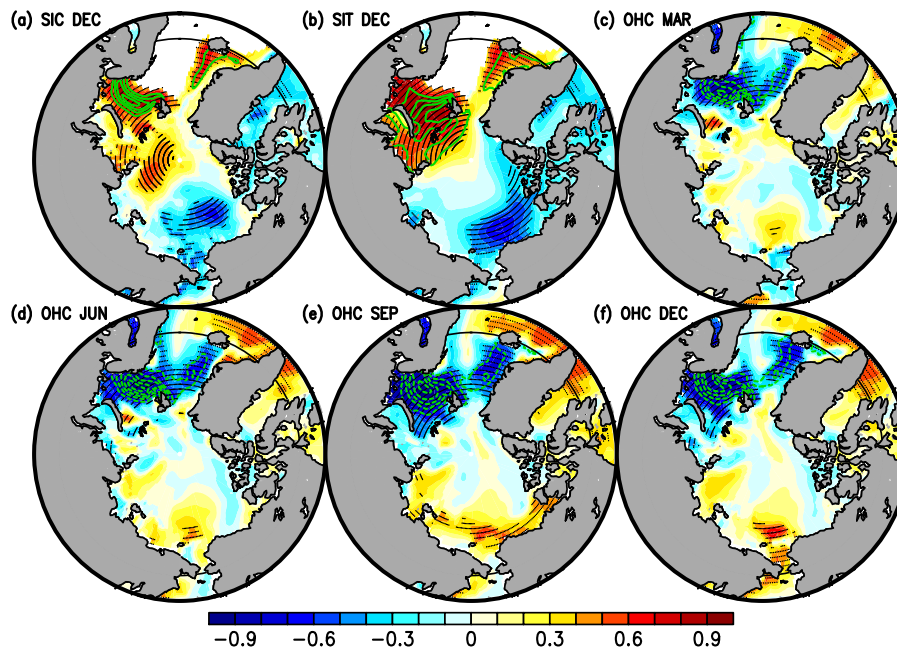
Figure 4. Lagged correlation (colours) and regression (contours) coefficients between the SIE_{AO} anomaly ($\times 10^6$ km^2) in December and **(a)** SIC anomaly (%) at a lag of 0 months, **(b)** SIT anomaly (cm) at a lag of 0 months, and OHC anomalies ($\times 10^{18}$ J) at lags of **(c)** -9, **(d)** -6, **(e)** -3, and **(f)** 0 months, in regions from 60 to 90° N on the basis of the hindcasts started from 1 January. Contours are drawn at intervals of 5 (%) from 5 to 25 for SIC and 10 (cm) from 10 to 40 for SIT. In **(c–f)**, the contours are drawn from -1.0 to -0.1 ($\times 10^{18}$ J) at intervals of 0.1 ($\times 10^{18}$ J). Stippling indicates regions with statistically significant correlation coefficients at the 95 % confidence level. White shading indicates areas where sea ice does not exist. A latitude circle of 65° N is also indicated by a thin solid line.
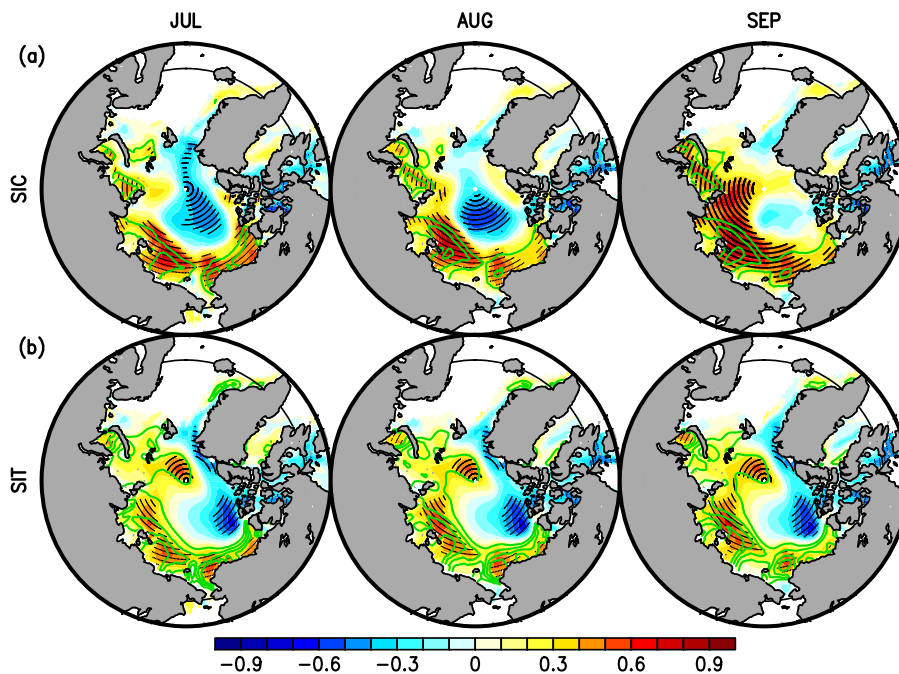
Figure 5. Lagged correlation (colours) and regression (contours) coefficients between the September SIE_{AO} anomaly ($\times 10^6$ km^2) and **(a)** SIC anomaly (%) and **(b)** SIT anomaly (cm), based on the hindcasts started from 1 July. Contours are drawn at intervals of 5 (%) from 5 to 20 and at intervals of 10 (cm) from 10 to 40 for the SIC and SIT anomalies, respectively. Stippling indicates regions with statistically significant correlation coefficients at the 95 % confidence level. White shading indicates areas where sea ice does not exist. A latitude circle of 65° N is also indicated by a thin solid line.

casts using an initialised climate model, MIROC5, and further identified physical processes related to the prediction skill. Prediction skill for Arctic winter SIE_{AO} is significantly higher than the persistence forecast, especially for December, indicating the possibility for dynamical forecasting 11 months ahead. The December SIE_{AO} is significantly correlated with the December SIC and SIT in the BS where the subsurface OHC anomalies might be advected from the North Atlantic, and subsequently emerge at the surface in winter, and contribute to the sea ice variability there. Our results suggest that the sources of the December SIE_{AO} prediction skill exist in the North Atlantic and thus initialisation of the subsurface water there leads to better prediction of the SIE_{AO} in December. Numerical experiments to confirm whether the subsurface OHC anomalies originating from the North Atlantic control the December sea ice extent in the BS and eventually in the Arctic Ocean will be explored in future work.

Significant skill for the September SIE_{AO} is seen only up to two months ahead. Improvement in the prediction skill for summer SIE_{AO} is dependent upon refinement of the initial state of the SIT. In fact, higher lagged correlations between the summer SIE_{AO} and the SIV_{AO} suggest that the initialisation of the SIT is important, which is consistent with previous results by Day et al. (2014a) and Bushuk et al. (2017).

In recent years, the rapid reduction in Arctic sea ice has enabled ships to navigate the Northern Sea Route (e.g., Stephenson et al., 2014). Under such maritime activities in the Arctic Ocean, forecasts of the local sea ice distribution rather than the total sea ice extent become of greater interest for marine users. Recent studies have reported the forecast skills of the retreat and advance dates of the sea ice distribution based on statistical methods (e.g., Stroeve et al., 2016; Wang et al., 2016) as well as a dynamical forecast system (Sigmond et al., 2016; Bushuk et al., 2017). In the present study, our hindcasts could not reproduce precise sea-ice edges from summer to fall. For example, the predicted sea ice distributions in September 2007 are overestimated in the Russian region of the Arctic Ocean. This is because the surface winds, which are thought to be the major driving force of sea ice motion in September 2007, are not adequately predicted. Other reasons might be the lower resolution of the ocean model or bias in the climatology. Further improvements in the skill to predict sea ice, including its spatial pattern, will be provided by climate models with higher resolution, reduced model drift and bias, and improved initialisation techniques.

References

Aksenov, Y., Ivanov, V. V., Nurser, A. J. G., Bacon, S., Polyakov, I. V., Coward, A. C., Naveira-Garabato, A. C., and Beszczynska-Moeller, A.: The Arctic circumpolar boundary current, J. Geophys. Res., 116, C09017, https://doi.org/10.1029/2010JC006637, 2011.

Armstrong, R. L., Knowles, K. W., Brodzik, M. J., and Hardman, M. A.: DMSP SSM/I-SSMIS Pathfinder daily EASE-grid brightness temperatures, Jan 1987–Dec 2011, National Snow and Ice Data Center, CO, digital media, available at: http://nsidc.org/data/nsidc-0032.html (last access: 27 November 2012), 2012.

National Snow and Ice Data Center: Arctic Sea Ice News & Analysis, available at: http://nsidc.org/arcticseaicenews/, last access: 7 September 2016.

Barnes, E. A. and Screen, J. A.: The impact of Arctic warming on the midlatitudes jet-stream: Can it? Has it? Will it?, WIREs Clim Change 2015, 6, 277–286, https://doi.org/10.1002/wcc.337, 2015.

Bekryaev, R. V., Polyakov, I. V., and Alexeev, V. A.: Role of polar amplification in long-term surface air temperature variations and modern Arctic warming, J. Clim., 23, 3888–3906, https://doi.org/10.1175/2010JCLI3297.1, 2010.

Bitz, C. M. and Lipscomb, W. H.: An energy-conserving thermodynamic model of sea ice, J. Geophys. Res., 104, 15669–15677, 1999.

Bitz, C. M., Holland, M. M., Weaver, A. J., and Eby, M.: Simulating the ice-thickness distribution in a coupled climate model, J. Geophys. Res., 106, 2441–2463, 2001.

Blanchard-Wrigglesworth, E., Bitz, C. M., and Holland, M. M.: Influence of initial conditions and climate forcing on predicting Arctic sea ice, Geophys. Res. Lett., 38, L18503, https://doi.org/10.1029/2011GL048807, 2011a.

Blanchard-Wrigglesworth, E., Armour, K. C., Bitz, C. M., and DeWeaver, E.: Persistence and inherent predictability of Arctic sea ice in a GCM ensemble and observations, J. Clim., 24, 231–250, https://doi.org/10.1175/2010JCLI3775.1, 2011b.

Bushuk, M., Msadek, R., Winton, M., Vecchi, G. A., Gudgel, R., Rosati, A., and Yang, X.: Skillful regional prediction of Arctic

sea ice on seasonal timescales, Geophys. Res. Lett., 44, 4953–4964, https://doi.org/10.1002/2017GL073155, 2017.

Chevallier, M. and Salas y Mélia, D.: The role of sea ice thickness distribution in the Arctic sea ice potential predictability: A diagnostic approach with a coupled GCM, J. Clim., 25, 3025–3038, https://doi.org/10.1175/JCLI-D-11-00209.1, 2012.

Chevallier, M., Salas y Mélia, D., Voldoire, A., and Déqué, M.: Seasonal forecasts of the Pan-Arctic sea ice extent using a GCM-based seasonal prediction system, J. Clim., 26, 6092–6104, https://doi.org/10.1175/JCLI-D-12-00612.1, 2013.

Cohen, J., Screen, J. A., Furtado, J. C., Barlow, M., Whittleston, D., Coumou, D., Franics, J., Dethloff, K., Entekhabi, D., Overland, J., and Jones, J.: Recent Arctic amplification and extreme mid-latitude weather, Nat. Geosci., 7, 627–637, https://doi.org/10.1038/NGEO2234, 2014.

Day, J. J., Hawkins, E., and Tietsche, S.: Will Arctic sea ice thickness initialization improve seasonal forecast skill?, Geophys. Res. Lett., 41, 7566–7575, https://doi.org/10.1002/2014GL061694, 2014a.

Day, J. J., Tietsche, S., and Hawkins, E.: Pan-Arctic and regional sea ice predictability: Initialization month dependence, J. Clim., 27, 4371–4390, https://doi.org/10.1175/JCLI-D-13-00614.1, 2014b.

Day, J. J., Tietsche, S., Collins, M., Goessling, H. F., Guemas, V., Guillory, A., Hurlin, W. J., Ishii, M., Keeley, S. P. E., Matei, D., Msadek, R., Sigmond, M., Tatebe, H., and Hawkins, E.: The Arctic Predictability and Prediction on Seasonal-to-Interannual TimEscales (APPOSITE) data set version 1, Geosci. Model Dev., 9, 2255–2270, https://doi.org/10.5194/gmd-9-2255-2016, 2016.

Guemas, V., Blanchard-Wrigglesworth, E., Chevallier, M., Day, J. J., Déqué, M., Doblas-Reyes, F. J., Fučkar, N. S., Germe, A., Hawkins, E., Keeley, S., Koenigk, T., Salas y Mélia, D., and Tietsche, S.: A review on Arctic sea-ice predictability and prediction on seasonal to decadal time-scales, Q. J. Roy. Meteorol. Soc., 142, 546–561, https://doi.org/10.1002/qj.2401, 2014.

Guemas, V., Chevallier, M., Déqué, M., Bellprat, O., and Doblas-Reyes, F.: Impact of sea ice initialization on sea ice and atmosphere prediction skill on seasonal timescales, Geophys. Res. Lett., 43, 3889–3896, https://doi.org/10.1002/2015GL066626, 2016.

Hirahara, S., Ishii, M., and Fukuda, Y.: Centennial-scale sea surface temperature analysis and its uncertainty, J. Clim., 27, 57–75, https://doi.org/10.1175/JCLI-D-12-00837.1, 2014.

Hunke, E. C. and Dukowicz, J. K.: An elastic-viscous-plastic model for sea ice dynamics, J. Phys. Oceanogr., 27, 1849–1867, 1997.

International CLIVAR Project Office: Decadal and bias correction for decadal climate predictions, International CLIVAR Project Office, CLIVAR Publication Series No. 150 (not peer reviewed), 2011.

IPCC: Climate Change 2013: The Physical Science Basis. Contribution of Working Group I to the Fifth Assessment Report of the Intergovernmental Panel on Climate Change, edited by: Stocker, T. F., Qin, D., Plattner, G.-K., Tignor, M., Allen, S. K., Boschung, J., Nauels, A., Xia, Y., Bex, V., and Midgley, P. M., Cambridge University Press, Cambridge, United Kingdom and New York, NY, USA, 1535 pp., https://doi.org/10.1017/CBO9781107415324, 2013.

Ishii, M. and Kimoto, M.: Reevaluation of historical ocean heat content variations with time-varying XBT and MBT depth bias corrections, J. Oceanogr., 65, 287–299, https://doi.org/10.1007/s10872-009-0027-7, 2009.

Ishii, M., Shouji, A., Sugimoto, S., and Matsumoto, T.: Objective analyses of sea-surface temperature and marine meteorological variables for the 20th century using ICOADS and the Kobe Collection, Int. J. Climatol., 25, 865–879, https://doi.org/10.1002/joc.1169, 2005.

Ishii, M., Kimoto, M., Sakamoto, K., and Iwasaki, S.-I.: Steric sea level changes estimated from historical ocean subsurface temperature and salinity analyses, J. Oceanogr., 62, 155–170, https://doi.org/10.1007/s10872-006-0041-y, 2006.

Kobayashi, S., Ota, Y., Harada, Y., Ebita, A., Moriya, M., Onoda, H., Onogi, K., Kamahori, H., Kobayashi, C., Endo, H., Miyaoka, K., and Takahashi, K.: The JRA-55 Reanalysis: General specifications and basic characteristics, J. Meteorol. Soc. Jpn., 93, 5–48, https://doi.org/10.2151/jmsj.2015-001, 2015.

Komuro, Y., Suzuki, T., Sakamoto, T. T., Hasumi, H., Ishii, M., Watanabe, M., Nozawa, T., Yokohata, T., Nishimura, T., Ogochi, K., Emori, S., and Kimoto, M.: Sea-ice in twentieth-century simulations by new MIROC coupled models: A comparison between models with high resolution and with ice thickness distribution, J. Meteorol. Soc. Jpn., 90A, 213–232, https://doi.org/10.2151/jmsj.2012-A11, 2012.

Kwok, R., Cunningham, G. F., Wensnahan, M., Rigor, I., Zwally, H. J., and Yi, D.: Thinning and volume loss of the Arctic Ocean sea ice cover: 2003–2008, J. Geophys. Res., 114, C07005, https://doi.org/10.1029/2009JC005312, 2009.

Lindsay, R. and Schweiger, A.: Arctic sea ice thickness loss determined using subsurface, aircraft, and satellite observations, The Cryosphere, 9, 269–283, https://doi.org/10.5194/tc-9-269-2015, 2015.

Lindsay, R. and Zhang, J.: Assimilation of ice concentration in an ice-ocean model, J. Atmos. Oceanic Tech., 23, 742–749, 2006.

Mori, M., Watanabe, M., Shiogama, H., Inoue, J., and Kimoto, M.: Robust Arctic sea-ice influence on the frequent Eurasian cold winters in past decades, Nat. Geosci., 7, 869–873, https://doi.org/10.1038/NGEO2277, 2014.

Msadek, R., Vecchi, G. A., Winton, M., and Gudgel, R. G.: Importance of initial conditions in seasonal predictions of Arctic sea ice extent, Geophys. Res. Lett., 41, 5208–5215, https://doi.org/10.1002/2014GL060799, 2014.

Nakanowatari, T., Sato, K., and Inoue, J.: Predictability of the Barents sea ice in early winter: Remote effects of oceanic and atmospheric thermal conditions from the North Atlantic, J. Clim., 27, 8884–8901, https://doi.org/10.1175/JCLI-D-14-00125.1, 2014.

Peterson, K. A., Arribas, A., Hewitt, H. T., Keen, A. B., Lea, D. J., and McLaren, A. J.: Assessing the forecast skill of Arctic sea ice extent in the GloSea4 seasonal prediction system, Clim Dyn., 44, 147–162, https://doi.org/10.1007/s00382-014-2190-9, 2015.

Pithan, F. and Mauritsen, T.: Arctic amplification dominated by temperature feedbacks in contemporary climate models, Nat. Geosci., 7, 181–184, https://doi.org/10.1038/NGEO2071, 2014.

Polyakov, I. V., Beszczynska, A., Carmack, E. C., Dmitrenko, I. A., Fahrbach, E., Frolov, I. E., Gerdes, R., Hansen, E., Holfort, J., Ivanov, V. V., Johnson, M. A., Karcher, M., Kauker, F., Morison, J., Orvik, K. A., Schauer, U., Simmons, H. L., Skagseth, Ø., Sokolov, V. T., Steele, M., Timokhov, L. A., Walsh, D., and Walsh, J. E.: One more step toward a warmer Arctic, Geophys.

Res. Lett., 32, L17605, https://doi.org/10.1029/2005GL023740, 2005.

Polyakov, I. V., Walsh, J. E., and Kwok, R.: Recent changes of arctic multiyear sea ice coverage and the likely causes, B. Am. Meteor. Soc., 93, 145–151, https://doi.org/10.1175/BAMS-D-11-00070.1, 2012.

Sigmond, M., Fyfe, J. C., Flato, G. M., Kharin, V. V., and Merryfield, W. J.: Seasonal forecast skill of Arctic sea ice area in a dynamical forecast system, Geophys. Res. Lett., 40, 529–534, https://doi.org/10.1002/grl.50129, 2013.

Sigmond, M., Reader, M. C., Flato, G. M., Merryfield, W. J., and Tivy, A.: Skillful seasonal forecasts of Arctic sea ice retreat and advance dates in a dynamical forecasts system, Geophys. Res. Lett., 43, 12457–12465, https://doi.org/10.1002/2016GL071396, 2016.

Smedsrud, L. H., Esau, I., Ingvaldsen, R. B., Eldevik, T., Haugan, P. M., Li, C., Lien, V. S., Olsen, A., Omar, A. M., Otterå, O. H., Risebrobakken, B., Sandø, A. B., Semenov, V. A., and Sorokina, S. A.: The role of the Barents Sea in the Arctic climate system, Rev. Geophys., 51, 415–449, https://doi.org/10.1002/rog.20017, 2013.

Stark, J. D., Ridley, J., Martin, M., and Hines, A.: Sea ice concentration and motion assimilation in a sea ice-ocean model, J. Geophys. Res., 113, C05S91, https://doi.org/10.1029/2007JC004224, 2008.

Stephenson, S. R., Brigham, L. W., and Smith, L. C.: Marine accessibility along Russia's Northern Sea Route, Polar Geogr., 37, 111–133, https://doi.org/10.1080/1088937X.2013.845859, 2014.

Stroeve, J. C., Crawford, A. D., and Stammerjohn, S.: Using timing of ice retreat to predict timing of fall freeze-up in the Arctic, Geophys. Res. Lett., 43, 6332–6340, https://doi.org/10.1002/2016GL069314, 2016.

Tatebe, H., Ishii, M., Mochizuki, T., Chikamoto, Y., Sakamoto, T. T., Komuro, Y., Mori, M., Yasunaka, S., Watanabe, M., Ogochi, K., Suzuki, T., Nishimura, T., and Kimoto, M.: The initialization of the MIROC climate models with hydographic data assimilation for decadal prediction, J. Meteorol. Soc. Jpn., 90A, 275–294, https://doi.org/10.2151/jmsj.2012-A14, 2012.

Tietsche, S., Day, J. J., Guemas, V., Hurlin, W. J., Keeley, S. P. E., Matei, D., Msadek, R., Collins, M., and Hawkins, E.: Seasonal to interannual Arctic sea ice predictability in current global climate models, Geophys. Res. Lett., 41, 1035–1043, https://doi.org/10.1002/2013GL058755, 2014.

Wang, L., Yuan, X., Ting, M., and Li, C.: Predicting summer Arctic sea ice concentration intraseasonal variability using a vector autoregressive model, J. Clim., 29, 1529–1543, https://doi.org/10.1175/JCLI-D-15-0313.1, 2016.

Wang, W., Chen, M., and Kumar, A.: Seasonal prediction of Arctic sea ice extent from a coupled dynamical forecast system, Mon. Weather Rev., 141, 1375–1394, https://doi.org/10.1175/MWR-D-12-00057.1, 2013.

Watanabe, M., Suzuki, T., O'ishi, R., Komuro, Y., Watanabe, S., Emori, S., Takemura, T., Chikira, M., Ogura, T., Sekiguchi, M., Takata, K., Yamazaki, D., Yokohata, T., Nozawa, T., Hasumi, H., Tatebe, H., and Kimoto, M.: Improved climate simulation by MIROC5: Mean states, variability, and climate sensitivity, J. Clim., 23, 6312–6335, https://doi.org/10.1175/2010JCLI3679.1, 2010.